Journal of Japan Association for Earthquake Engineering, Vol. 23, No. 6, 2023

A PROPOSAL OF THE SCALING RELATION FOR THE SHORT-PERIOD LEVEL ASSOCIATED WITH THE THREE-STAGE MODEL OF INLAND CRUSTAL EARTHQUAKES

Masanobu TOHDO[1], Kensuke ARAI[2], Jun'ichi MIYAKOSHI[3], Toshiaki SATO[4], Hiroyuki FUJIWARA[5] and Nobuyuki MORIKAWA [6]

[1] Member, Dr. Eng., Principal Researcher, Ohsaki Research Institute, Inc., Tokyo, Japan, tohdo@ohsaki.co.jp
[2] Member, M. Eng., Senior Researcher, Ohsaki Research Institute, Inc., Tokyo, Japan, arai@ohsaki.co.jp
[3] Member, Dr. Eng., Research Director, Ohsaki Research Institute, Inc., Tokyo, Japan, miya@ohsaki.co.jp
[4] Member, Dr. Eng., Director, Ohsaki Research Institute, Inc., Tokyo, Japan, satom@ohsaki.co.jp
[5] Member, Dr. Sc., Director, National Research Institute for Earth Science and Disaster Resilience, Ibaraki, Japan, fujiwara@bosai.go.jp
[6] Member, Dr. Sc., Chief Researcher, National Research Institute for Earth Science and Disaster Resilience, Ibaraki, Japan, morikawa@bosai.go.jp

ABSTRACT: We re-examined the empirical scaling relationship between seismic moment M_0 and short-period level A, which is the flat level of the acceleration source spectrum, adopted for setting asperity models of the inland crustal earthquakes in the "Recipe" for predicting strong ground motions published by the Headquarters for Earthquake Research Promotion (2020). Taking into consideration the scaling relationship between seismic moment and rupture area, which is defined as the three-stage model in the Recipe, an empirical equation was newly proposed as a three-fold-line model in which the short-period level was scaled with $M_0^{1/3}$, $M_0^{1/4}$, and $M_0^{1/2}$ for each stage of the three-stage model. By comparing this new empirical equation with the data obtained from earthquake observation records, which included the area and stress drop of the strong motion generation area (SMGA), we found that the three-fold-line model for short-period level could match the short-period level data of SMGAs, and that the stress drop calculated from the empirical equation is independent of the seismic moment, which is consistent with the observational stress drop data of SMGAs.

Keywords: *Inland crustal earthquake, Short-period level, Scaling relation, Recipe, Asperity model, Three-stage model*

1. INTRODUCTION

The "Recipe"[1] published by the Headquarters for Earthquake Research Promotion (HERP) plays an important role in the evaluation of a fault model for predicting strong ground motions. Among the asperity models used in the Recipe, this study examines the inland crustal earthquakes that occur on active faults. Two factors are considered important in the Recipe: M_0–S, which is the scaling relationship between the seismic moment M_0 and fault area S for outer fault parameters; M_0–A, which is the scaling relationship between M_0 and short-period level A, which is closely related to the area and stress drop on asperities for inner fault parameters, which in turn have a large influence on strong ground motions. The short-period level represents a flat level in the high-frequency range of the acceleration source spectrum. The empirical equations based on the analyses of earthquake observation records play an important role while setting these fault parameters.

The M_0–S scaling law for inland crustal earthquakes in the Recipe is represented by the three-stage model (Irikura and Miyake[2]) with different scaling slopes on M_0. The empirical equations proposed by Somerville et al.[3], Irikura and Miyake[4], and Murotani et al.[5] were applied to the seismic moment region of each stage, and the fault area S was scaled by $M_0^{2/3}$, $M_0^{1/2}$, and M_0^{1}, respectively. The empirical equation proposed by Dan et al.[6] was applied for a short-period level A of inland crustal earthquakes in the Recipe. In the M_0–A relationship presented in this equation, the short-period level was scaled by $M_0^{1/3}$. When the asperity area, S_{asp} and the stress drop on asperities, $\Delta\sigma_{asp}$ are calculated by the method proposed in the Recipe by applying these empirical equations, the ratio of asperity area to the fault area, S_{asp}/S and $\Delta\sigma_{asp}$ of asperities are constant values independent of the seismic moment in the first stage. However, a relationship dependent on the seismic moment for those parameters is obtained in the second stage and thereafter[7].

Studies have been conducted on the scaling law of the area of asperity, S_{asp}, based on the heterogeneous slip distribution of the source inversion results using earthquake observation records of inland crustal earthquakes. In a pioneering study by Somerville et al.[3], S_{asp} was scaled with respect to the seismic moment M_0 using $M_0^{2/3}$ as the fault area S. In their study, the relationship between S_{asp}/S and M_0 was unclear and the average value of S_{asp}/S data was 0.22. Tajima et al.[8] on great inland crustal earthquakes (M_W 7.5~7.9) and Nagashima et al.[9] on many overseas inland crustal earthquakes (M_W 4.5~8.0) showed that the area ratio, S_{asp}/S can be 0.22 on an average regardless of the magnitude of the earthquake. Miyakoshi et al.[10), 11] studied the scaling law of the area of asperity, S_{asp} of inland crustal earthquakes in Japan and showed that S_{asp} can be scaled with $M_0^{2/3}$ as proposed by Somerville et al.[3]. Furthermore, Miyakoshi et al.[11] inferred that when M_0 increases, S_{asp} bends at M_W6.5 and is proportional to $M_0^{1/2}$. The scaling slope of S_{asp} on M_0 above M_W6.5 is similar to the scaling relationship of M_0-S in the second stage proposed by Irikura and Miyake[4]. Based on these studies, the area ratio of the asperity, S_{asp}/S can be considered as a parameter independent of M_0.

Studies have been conducted on the parameters of the strong motion generation area (SMGA)[12] estimated from the simulation analyses of strong ground motion records of inland crustal earthquakes. Tajima et al.[8] and Miyakoshi et al.[10] showed that the area of SMGA was almost the same as S_{asp} based on the heterogeneous slip distribution, as pointed out by Miyake et al.[12]. In other words, the area of SMGA can be considered equivalent to S_{asp}. In addition, the stress drop on SMGA, which can simulate strong ground motion records, can be considered to be equivalent to the stress drop of asperity $\Delta\sigma_{asp}$. Miyakoshi et al.[10] showed that the stress drop of SMGA and $\Delta\sigma_{asp}$ correspond to each other, and that the mean values of the two are almost identical. This was studied regardless of the seismic moment M_0, further indicating that the stress drop of SMGA can be poorly correlated with M_0[13].

As described above, in the method for evaluating the fault model of the Recipe (described in detail in Section 2), the asperity area ratio S_{asp}/S and stress drop on asperity depend on the earthquake scale (seismic moment M_0) after the second stage[7], whereas the analysis results of earthquake observation records[3), 8)-11] do not tend to depend on the earthquake scale for the area ratio S_{asp}/S and stress drop on asperity. Therefore, in this study, we re-examined the scaling relationship of M_0–A between the seismic moment M_0 and short-period level A, which can evaluate the stress drop of asperity according to the characteristic that it does not depend on the earthquake scale.

There are studies by Dan et al.[7), 14)] and Hikima and Shimmura[15), 16)] on scaling, in which the average stress drop of the entire fault $\Delta\sigma$ and the stress drop of asperity $\Delta\sigma_{asp}$ are constant over a wide range of earthquake magnitude scales, and as a result, the asperity area ratio, S_{asp}/S becomes constant. In these studies, they first set an equation to evaluate $\Delta\sigma$ from M_0 and S. Thereafter, based on the equation, they constructed the scaling law of M_0–S by giving a certain $\Delta\sigma$ that matches the earthquake data of M_0 and S. Then, the stress drop on asperity, $\Delta\sigma_{asp}$ was provided to match the short-period level of earthquake data. The difference between the previous studies and this study is that here, we used a method for evaluating the asperity parameters based on the M_0–S scaling law of the three-stage model in the Recipe, whereas the previous studies are based on a different M_0–S scaling law.

Section 2 details the method in the Recipe for setting fault parameters based on the three-stage model, and thereafter, summarizes the relationship between seismic moment and asperity parameters (area and stress drop) evaluated by the method. In Section 3, we first review previous research based on source inversion analyses. Thereafter, we consider the scaling of the short-period level derived from the area and stress drop on asperity, and thereafter, construct a new scaling law for M_0–A relations from the

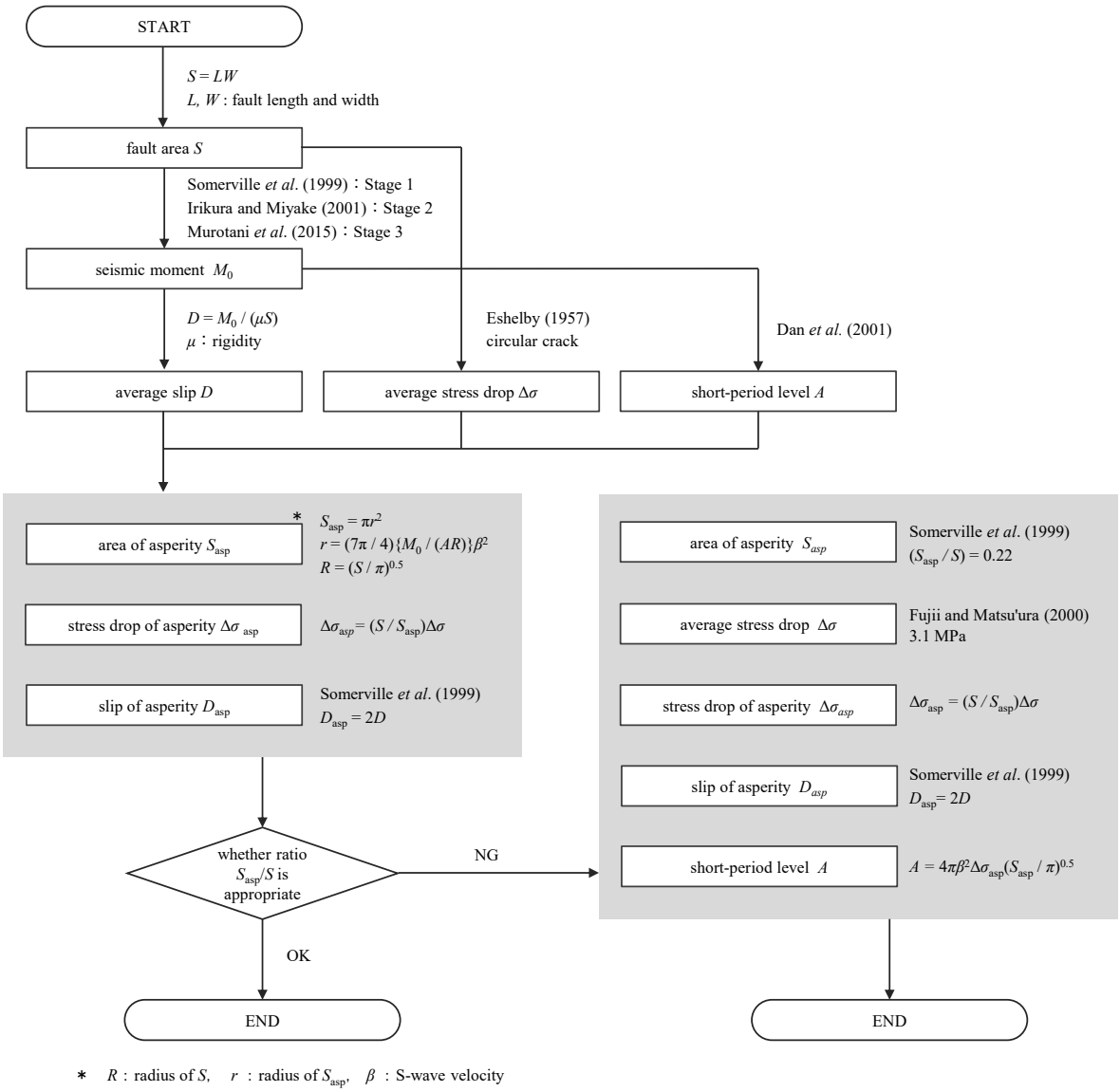

Fig. 1 Flowchart for setting the main fault parameters of inland crustal earthquakes in the Recipe[1)] by HERP

least-squares method using the short-period level data reported by Dan et al. [6]. Section 4 verifies the validity of the new scaling law of the M_0–A relationship by comparing it with the short-period level data of the SMGA obtained from the waveform inversion. Furthermore, we compared the stress drop estimated from the new scaling law of M_0–A with the stress drop data of SMGA.

2. METHOD FOR SETTING THE FAULT PARAMETERS IN THE RECIPE BY HERP

The fault parameters of inland crustal earthquakes were set according to the Recipe by considering the fault area as the basic quantity. A flowchart indicating the main fault parameters is depicted in Fig. 1. It should be noted that, in addition to the asperity, the background region that bears a certain part of the seismic moment is required for the asperity model, but the explanation for the background region is omitted in Fig. 1.

The empirical relationship between the fault area and seismic moment in the Recipe was evaluated using the three-stage model (Irikura and Miyake[2]) based on whether the rupture of a fault reaches the surface layer or not; and whether the slip of a fault is saturated or not. Figure 2 depicts the schematic of source model of the three-stage model. In the first stage, the seismic moment is proportional to the 1.5th power of the fault area because the fault length, fault width, and average slip are proportional to $M_0^{1/3}$. In the second stage, the seismic moment is proportional to the square of the fault area because the fault width, W_{max} saturated with the seismogenic zone. In the third stage, the average slip is saturated to a constant value of D_{max}, such that the seismic moment is proportional to the fault area. Based on these considerations, the empirical equation indicating the relationship between the seismic moment M_0 (Nm) and fault area S (km^2) of the three-stage model is as follows:

$$M_0 = \begin{cases} \left(\dfrac{S}{2.23}\times 10^{15}\right)^{3/2}\times 10^{-7} & , \quad M_0 < 7.5\times 10^{18} \\ \left(\dfrac{S}{4.24}\times 10^{11}\right)^{2}\times 10^{-7} & , \quad 7.5\times 10^{18} \le M_0 \le 1.8\times 10^{20} \\ S\times 10^{17} & , \quad M_0 > 1.8\times 10^{20} \end{cases} \tag{1}$$

The first, second, and third statements in Eq. (1) are the empirical equations proposed by Somerville et al.[3], Irikura and Miyake[4], and Murotani et al.[5], respectively. These equations are based on Eq. (2), and was used to evaluate S (km^2) from M_0 (Nm).

$$S = \begin{cases} 2.23\times 10^{-15}\times\left(M_0\times 10^{7}\right)^{2/3} & , \quad M_0 < 7.5\times 10^{18} \\ 4.24\times 10^{-11}\times\left(M_0\times 10^{7}\right)^{1/2} & , \quad 7.5\times 10^{18} \le M_0 \le 1.8\times 10^{20} \\ 1.0\times 10^{-17}\times M_0 & , \quad M_0 > 1.8\times 10^{20} \end{cases} \tag{2}$$

In Eqs. (1) and (2), the range of seismic moments corresponding to each equation is shown. However, as described in the Recipe, it is more rational to use each equation according to the concept of modeling the seismic source, as depicted in Fig. 2.

Short-period level A was applied to determine the area and stress drop of asperity and was evaluated using the following empirical Eq. (3), as proposed by Dan et al.[6] from the seismic moment M_0:

$$A = 2.46\times 10^{10}\times\left(M_0\times 10^{7}\right)^{1/3} \tag{3}$$

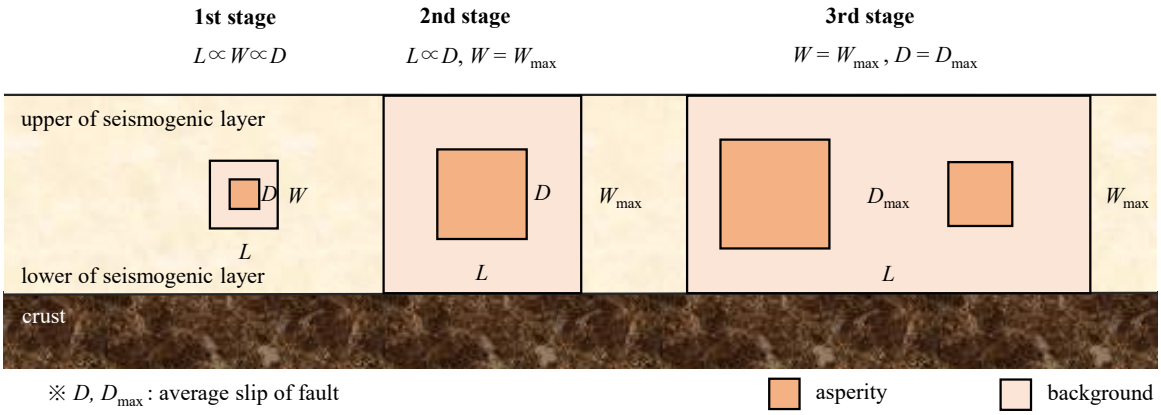

Fig. 2 Schematic source model of the three-stage model for inland crustal earthquakes

where A is in Nm/s^2 and M_0 is in Nm.

The theoretical relationship of the short-period level composed of the asperity area, S_{asp} and stress drop on asperity, $\Delta\sigma_{asp}$ is expressed by Eq. (4). This equation was derived by Dan and Sato[17] based on the seismic source spectrum, which is the equation first proposed by Brune[18] and later, expanded for the asperity model by Boatwright[19] .

$$A = 4\pi \cdot \beta^2 \cdot \Delta\sigma_{asp} \sqrt{S_{asp} / \pi} \tag{4}$$

where β is the S-wave velocity at source. In Eq. (4), the short-period level from the background was not considered as it was sufficiently small.

Using Eq. (4), the ratio of asperity area to fault area, S_{asp}/S can be expressed using Eq. (5)[7], by applying the equation for the average stress drop $\Delta\sigma$ in the circular crack proposed by Eshelby[20], and the equation proposed by Madariaga[21] (Eq. (12) described below) which shows the relationship between $\Delta\sigma$ and $\Delta\sigma_{asp}$ by considering each area.

$$\frac{S_{asp}}{S} = \left\{ \frac{7\pi^2 \beta^2 M_0}{4AS} \right\}^2 \tag{5}$$

The stress drop of asperity $\Delta\sigma_{asp}$ can be expressed by applying Eq. (4) and Eq. (5) to Eq. (6).

$$\Delta\sigma_{asp} = \frac{A^2 S^{1/2}}{7\pi^{5/2} \beta^4 M_0} \tag{6}$$

According to the flowchart depicted in Fig. 1, if Eqs.(5) and (6) are expressed as functions of M_0 using the empirical equations of M_0–S by Eq. (1), and M_0–A by Eq. (3), $\Delta\sigma$ and $\Delta\sigma_{asp}$ become constant values from the scaling relationship of self-similarity[4] and M_0–A in the region of the first stage, and the ratio of asperity area to fault area, S_{asp}/S is also constant regardless of the seismic moment M_0. On the other hand, in the second stage, the stress drop of asperity $\Delta\sigma_{asp}$ is proportional to $M_0^{-1/12}$, and the area ratio of asperity S_{asp}/S is proportional to $M_0^{1/3}$, which is a relationship that depends on the earthquake scale (Dan et al.[7]). In particular, because S_{asp}/S is proportional to $M_0^{1/3}$, the area ratio S_{asp}/S for long faults with a fault area that exceeds approximately 1800 km^2 (approximately 1.8×10^{20} Nm in M_0) exceeds 0.5, and in that case, we cannot set up a fault model[7]. In the Recipe, if S_{asp}/S is more excessive than previous research results or an earthquake is in the third stage, $\Delta\sigma$, $\Delta\sigma_{asp}$ and S_{asp}/S are provided a

constant amount, respectively. Specifically, S_{asp}/S is provided as approximately 22% based on Somerville et al.[3] and $\Delta\sigma$ is given as 3.1 MPa with reference to Fujii and Matsu'ura[22], and the fault parameters are set from them. As a result, $\Delta\sigma_{asp}$ is approximately 14.4 MPa, which is roughly consistent with the previous research results. However, the 3.1 MPa by Fujii and Matsu'ura[22] was derived under limited conditions; therefore, the method is treated as a tentative method in the Recipe until new knowledge is obtained[1].

3. RECONSIDERATION OF THE SCALING LAW FOR THE SHORT-PERIOD LEVEL BY DAN ET AL. (2001)

3.1 Previous research on the asperity area and stress drop on asperity

In the Recipe method described in Section 2, during the second stage where the seismic moment M_0 is in the range of 7.5×10^{18} Nm $\leq M_0 \leq 1.8\times10^{20}$ Nm, $\Delta\sigma_{asp}$ and S_{asp}/S depend on M_0.

Here, we review the relationship between the area and stress drop on asperity and the seismic moment in previous studies based on the analysis of observation records of inland crustal earthquakes.

Somerville et al.[3] determined S and S_{asp} for 15 earthquakes in the range of 3.5×10^{17} Nm $\leq M_0 \leq 7.5\times10^{19}$ Nm by trimming the heterogeneous slip distribution based on the source inversion. Thereafter, these areas were scaled by the same $M_0^{2/3}$ for the seismic moment M_0 to obtain the empirical equations for S and S_{asp}. Consequently, S_{asp}/S was expressed as a constant ratio regardless of M_0, and the average value was 0.22.

Tajima et al.[8] examined the fault parameters of overseas large earthquakes in the range of 1.98×10^{20} Nm $\leq M_0 \leq 9.7\times10^{20}$ Nm. It was found that the asperity area obtained from the heterogeneous slip distribution and the area of SMGA S_{SMGA} estimated by the simulation analyses of strong ground motion records were almost the same, and the asperity area ratio was consistent with 0.22 as obtained by Somerville et al.[3].

Miyakoshi et al.[10] conducted a study on S and S_{asp} similar to that by Somerville et al.[3] for 18 earthquakes in the range of 1.31×10^{17} Nm $\leq M_0 \leq 3.3\times10^{19}$ Nm in Japan using the source inversion results from the observation records of the observation network (K-NET, KiK-net, etc.), and further analyzed the area and stress drop of the SMGA model. They compared the mean of the area ratio S_{asp}/S from the collected data with the area ratio of 0.22 by Somerville et al.[3], and also compared the mean of the stress drop of asperity and that from the SMGA data. These comparisons were based on the average values and were not related to the earthquake scale, indicating that the area ratio and stress drop of asperity are indirect parameters that do not depend on the earthquake scale. In their study[10], as pointed out by Miyake et al.[12], the area of the SMGA almost coincides with the area of asperity owing to the heterogeneous slip distribution, and the stress drop of SMGA $\Delta\sigma_{SMGA}$ was similar to the stress drop averaged in the asperity region. In this study, we consider that the area S_{SMGA} and stress drop of SMGA $\Delta\sigma_{SMGA}$ of inland crustal earthquakes are equivalent to S_{asp} and $\Delta\sigma_{asp}$ in the asperity model for strong ground motion prediction depicted in Fig. 1.

Miyakoshi et al.[11] examined waveform inversion results of 22 earthquakes (M_W 5.4~7.1) in Japan and found that the scaling slope of the asperity area S_{asp} with respect to the seismic moment M_0 is proportional to $M_0^{2/3}$ in accordance with the slope reported by Somerville et al.[3], and they inferred that the S_{asp} bends at M_W6.5 and is proportional to $M_0^{1/2}$ as it does in the second stage of Eq. (2) at M_W6.5 or higher.

Nagashima et al.[9] found that from a study using the source inversion results of a number of overseas inland crustal earthquakes in the range of 7.96×10^{15} Nm $\leq M_0 \leq 9.42\times10^{20}$ Nm, the asperity area scaled with respect to the seismic moment is consistent with the area obtained by multiplying the fault area from Eq. (2) by 0.22 times. The results showed that 22% of the fault area could be the average value of the asperity area, regardless of the earthquake scale.

Tohdo et al.[13] collected the stress drop and the area of SMGA data estimated by analyses of strong motion records of 12 earthquakes in the range of 7.5×10^{18} Nm $\leq M_0 \leq 1.10\times10^{21}$ Nm, including three overseas earthquakes, and stated that both the area ratio and stress drop of SMGA were poorly correlated

with the seismic moment.

As described above, the S_{asp}/S and $\Delta\sigma_{asp}$ obtained from the analyses of observed records of inland crustal earthquakes with wide scale of earthquake magnitude from the first stage to the third stage do not tend to depend on the earthquake scale. This tendency is not consistent with the dependence of the area ratio and stress drop on the asperity on the earthquake scale obtained from the Recipe method detailed in Section 2.

3.2 Formulation of the scaling law of the M_0–A relationship associated with the three-stage model

Based on the characteristics of the asperity parameters, which were obtained from the analyses of earthquake observation records from previous studies mentioned in Section 3.1, we reconsidered the scaling law for the short-period level with respect to the seismic moment according to the empirical relation of Eq. (3).

First, it is assumed that $\Delta\sigma_{asp}$ and S_{asp}/S can be expressed as constants regardless of the seismic moment M_0. The stress drop, which is assumed to be constant is $\Delta\sigma_{casp}$, and area ratio is s_{casp} as expressed in the following equation.

$$s_{casp} = \frac{S_{asp}}{S} = const. \tag{7}$$

Equation (4) can be rewritten using $\Delta\sigma_{casp}$ and s_{casp} to obtain Eq. (8) for evaluating the short-period level A with fault area S as a variable.

$$A = 4\pi \cdot \beta^2 \cdot \Delta\sigma_{casp} \sqrt{s_{casp}} \cdot \sqrt{S/\pi} \tag{8}$$

Now, let us consider the relationship between the short-period level and seismic moment, which can be expressed using Eq. (8), by associating it with the scaling law of the M_0–S relationship in Eq. (1) or Eq. (2) for the three-stage model in the Recipe[1]. Equation (8) indicates that the short-period level A can be expressed as the product of a constant and square root $S^{1/2}$ of the fault area S. Therefore, by considering that fault area S in the first, second, and third stages of Eq. (2) is proportional to $M_0^{2/3}$, $M_0^{1/2}$, and M_0^{1}, respectively, during each stage with the seismic moment M_0, the short-period level A for getting evaluated by M_0 needs to be scaled by $M_0^{1/3}$, $M_0^{1/4}$, and $M_0^{1/2}$ corresponding to the region of each stage of M_0 in the Recipe. Based on these considerations, the scaling relationship of M_0–A is set to Eq. (9), and the range of M_0 (Nm) during each stage is similar to that expressed in Eq. (1) or Eq. (2) in the Recipe:

$$A = \begin{cases} \alpha_1 \times M_0^{1/3} & , \quad M_0 < 7.5\times10^{18} \\ \alpha_2 \times M_0^{1/4} & , \quad 7.5\times10^{18} \le M_0 \le 1.8\times10^{20} \\ \alpha_3 \times M_0^{1/2} & , \quad M_0 > 1.8\times10^{20} \end{cases} \tag{9}$$

Here, α_1, α_2, and α_3 are the constants for each stage.

3.3 Setting the scaling law of the relationship of M_0–A using the data from Dan et al. (2001)

Equation (3) proposed by Dan et al.[6] corresponding to the scaling of $M_0^{1/3}$ in the first stage of Eq. (9) has been determined by applying the least-squares method by setting the scaling of $M_0^{1/3}$ to the short-period level data obtained from the source inversion results of 12 inland crustal earthquakes in the range of 3.5×10^{17} Nm $\le M_0 \le 7.5\times10^{19}$ Nm. In this study, we set the scaling of $M_0^{1/3}$, $M_0^{1/4}$, and $M_0^{1/2}$ during each stage of the three-stage model in the Recipe for the short-period level A, and determined the constants of Eq. (9) by applying the least-squares method to 12 data points, as performed by Dan et al.[6].

Herein, short-period level A is set to be continuous with respect to M_0 at the boundary $M_0 = 7.5\times10^{18}$

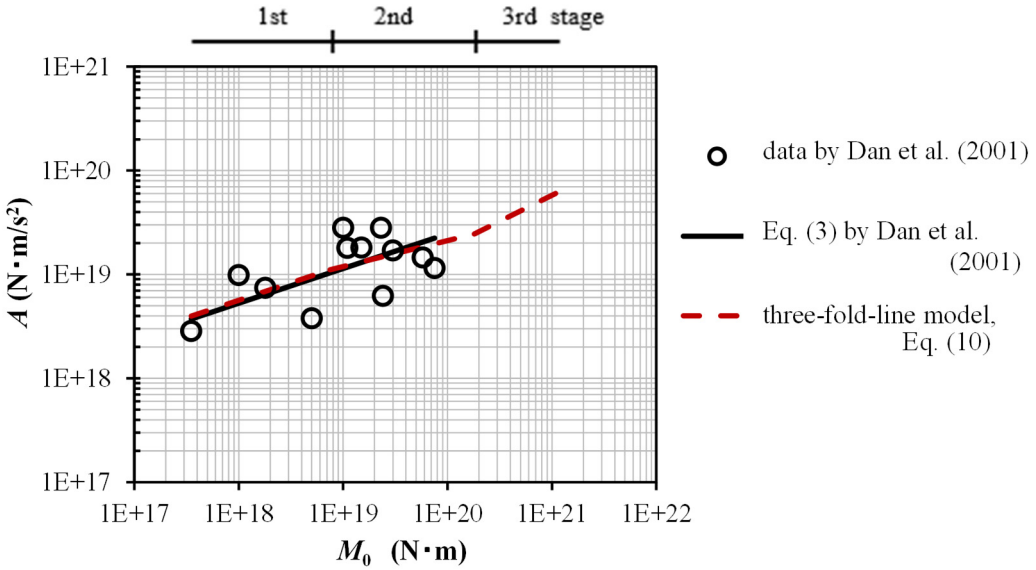

Fig. 3 Comparison of the M_0–A relationship between the seismic moment M_0 and the short-period level A by the three-fold-line model expressed using Eq. (10) with that of the 12 data used by Dan et al.[6], as well as the M_0–A relationship by Eq. (3)

Nm between the first and second stages and at the boundary $M_0 = 1.8\times10^{20}$ Nm between the second and third stages. Because there is only one unknown present in these conditions, it is determined by the least-squares method, in which the sum of the squares of the logarithmic errors of both the data and short-period level A estimated by Eq. (9) is minimized. Consequently, the M_0–A relationship between the seismic moment (M_0; Nm) and short-period level (A; Nm/s^2) in the first, second, and third stages becomes Eq. (10).

$$A = \begin{cases} 5.66\times10^{12}\times M_0^{1/3} & , \quad M_0 < 7.5\times10^{18} \\ 2.12\times10^{14}\times M_0^{1/4} & , \quad 7.5\times10^{18} \le M_0 \le 1.8\times10^{20} \\ 1.83\times10^{9}\times M_0^{1/2} & , \quad M_0 > 1.8\times10^{20} \end{cases} \tag{10}$$

Hereinafter, this result is called the three-fold-line model.

Figure 3 depicts the M_0–A relationship for the short-period level between the three-fold-line model expressed in Eq. (10) and 12 data points reported by Dan et al.[6] used for the least-squares method, as well as the M_0–A relationship by Eq. (3). By comparing short-period level A according to Eq. (3) and Eq. (10) in the range of seismic moment M_0 at 12 data points, the short-period level according to Eq. (10) was slightly larger (1.07 times) than that obtained using Eq. (3) in the first stage of $M_0 < 7.5\times10^{18}$ Nm. Then, in the range of seismic moment M_0 greater than 1.68×10^{19} Nm in the second stage, the short-period level A according to Eq. (10) becomes less than A using Eq. (3).

3.4 Stress drop of asperity estimated from the three-fold-line model

Here, let us discuss the stress drop on asperity obtained from the M_0–A relation expressed in Eq. (10). By assuming that the asperity area ratio S_{asp}/S to the fault area S can be expressed as a constant value s_{casp} as expressed in Eq. (7), the stress drop of asperity $\Delta\sigma_{asp}$ can be obtained using Eq. (11), based on Eq. (4).

$$\Delta\sigma_{asp} = \frac{A}{4\pi \cdot \beta^2 \cdot \sqrt{s_{casp}} \cdot \sqrt{S/\pi}} \tag{11}$$

Here, $\Delta\sigma_{asp}$ from the first stage to the third stage is obtained using Eq. (11), and area ratio s_{casp} used in Eq. (11) was set to 0.22 according to the Recipe. This is derived from the fact that S_{asp}/S according to Somerville et al.[3] is 0.22, regardless of the seismic moment. This area ratio was confirmed by the results studied by Tajima et al.[8] on earthquake data in the range of M_0 during the third stage and the results studied by Nagashima et al.[9] using several earthquake data in the range of M_0 from the first stage to the third stage, which were analyzed by applying the slip distributions of overseas inland crustal earthquakes by source inversion. However, Miyakoshi et al.[10] obtained results from the analyses of earthquake data in Japan, where the average area ratio S_{asp}/S of asperity is 0.16, which is smaller than 0.22. Therefore, future studies should accurately evaluate the area ratio $s_{casp} = S_{asp}/S$, which can set an appropriate asperity area S_{asp} corresponding to Eq. (11).

By substituting the short-period level A according to Eq. (10) of the three-fold-line model and fault area S using Eq. (2), for the three-stage model in Eq. (11), the stress drops of the asperity in the region of M_0 in the first, second, and third stages of the Recipe become constant stress drops of 14.0 MPa, 14.5 MPa, and 14.5 MPa, respectively. The S-wave velocity β in Eq. (11) was set to 3.46 km/s with reference to Dan et al.[7]. Next, as a reference, the average stress drop $\Delta\sigma$ of the entire fault was calculated using Eq. (12), considering the relationship by Madariaga[21] and the area ratio S_{asp}/S of 0.22 from the stress drop $\Delta\sigma_{asp}$ of asperity. It should be that $\Delta\sigma$ is not used to calculate $\Delta\sigma_{asp}$ as shown in Eq. (11); therefore, $\Delta\sigma$ in Eq. (12) is the reference value used in this study.

$$\Delta\sigma = \frac{\Delta\sigma_{asp} S_{asp}}{S} \tag{12}$$

As a result, the average stress drops $\Delta\sigma$ in each stage are 3.07 MPa, 3.20 MPa, and 3.20 MPa, respectively. These $\Delta\sigma$s are similar to 3 MPa reported by Hikima and Shimmura[15], corresponding to the earthquake data from the first to third stages, and 3.1 MPa reported by Fujii and Matsu'ura[22] and 3.4 MPa reported by Dan et al.[7] corresponding to the earthquake data of the second and third stages.

4. COMPARISON OF THE SHORT-PERIOD LEVEL OF THE THREE-FOLD-LINE MODEL AND STRONG MOTION GENERATION AREA DATA

4.1 Collection of strong motion generation area (SMGA) data

To examine the validity of the three-fold-line model using Eq. (10), which expresses the relationship between the seismic moment M_0 and short-period level A, we collected data on the area and stress drop of the SMGA, S_{SMGA} and $\Delta\sigma_{SMGA}$ of inland crustal earthquakes obtained by strong ground motion simulation in earthquake observation records. We also collected data on the seismic moment M_0 and fault area S of these earthquakes. Table 1 lists the source parameters of the 16 earthquakes. There were seven strike-slip fault earthquakes, eight reverse-slip fault earthquakes, and one normal slip fault earthquake. Seismic moments of earthquakes in Japan since 2000 have been published on F-net. The number of SMGAs in the citations of earthquakes No.5 and 15 was one, and number of SMGAs in the citations of other earthquakes was two to five. Table 1 lists the area S_{SMGA} and stress drop $\Delta\sigma_{SMGA}$ of the SMGA for each citation applied in this study. For citations with multiple SMGAs, the sum of their areas was used as the S_{SMGA}, and average of their stress drops weighted by each area of SMGAs was used as the stress drop $\Delta\sigma_{SMGA}$. For the short-period level A_{SMGA} of each citation listed in Table 1, the A_{SMGA} was obtained using Eq. (4) for each SMGA. In the case of citations with multiple SMGAs, the square root of the square-sum was used as the A_{SMGA} for our study. As for the S-wave velocity β used in Eq. (4), if β is specified in the cited reference, then that value is used. Else, when β is not specified, the value is

Table 1 The outer fault parameters and the parameters of the strong motion generation area (SMGA) for the collected 16 earthquakes of inland crustal earthquakes

Fault type	No.	Event	Outer fault parameters[*1]			SMGA parameters[*3]					
			Ref.	M_0[Nm]	S[km^2]	Ref.	S_{SMGA} [km^2]	$\Delta\sigma_{SMGA}$[MPa]	S_{SMGA}/S	β[km/s]	A_{SMGA}[Nm/s^2]
Strike-slip	1	1995 Hyogo-Ken Nanbu	5)	2.70×10^{19}	1,027	23)	304	10.2	0.30	3.5	1.62×10^{19}
						24)	337.28	10.7	0.33	3.5[*4]	1.83×10^{19}
						ave.	320.2	10.4	0.31	—	1.72×10^{19}
	2	1999 Kocaeli	5)	2.10×10^{20}	2,499	25)	584	10.8	0.23	3.5[*4]	2.31×10^{19}
	3	2000 Tottori-Ken Seibu	45)	8.62×10^{18}	598	26)	57.6	21.0	0.10	3.5	1.46×10^{19}
	4	2005 Fukuoka-Ken Seiho-Oki	46)	7.80×10^{18}	468	27)	156.25	11.3	0.33	3.46	1.20×10^{19}
	5	2013 Tochigi-Ken Hokubu	28)	5.54×10^{17}	84	28)	17.6	16.4	0.21	3.5[*4]	5.98×10^{18}
	6	2016 Kumamoto	29)	4.42×10^{19}	930	29)	203.6	13.5	0.22	3.4	1.58×10^{19}
						30)	351.36	11.5	0.38	3.5	1.87×10^{19}
						31)	220	8.9	0.24	3.4	1.14×10^{19}
						ave.	250.6	11.1	0.27	—	1.50×10^{19}
	7	2016 Tottori-Ken Chubu	47)	2.24×10^{18}	256	32)	50.9	12.7	0.20	3.5	8.08×10^{18}
Reverse-slip	8	1999 Chi-Chi	5)	3.50×10^{20}	3,435	25)	1020	10.0	0.30	3.5[*4]	2.77×10^{19}
	9	2004 Niigata-Ken Chuuetsu	48)	7.53×10^{18}	504	33)	91	9.3	0.18	3.5	8.72×10^{18}
						34)	90	14.7	0.18	3.5[*4]	1.26×10^{19}
						ave.	90.5	11.7	0.18	—	1.05×10^{19}
	10	2004 Rumoi	35)	4.44×10^{17}	100[*2]	35)	9.8	15.9	0.10	3.0	3.39×10^{18}
	11	2007 Noto-Hanto	10)	1.36×10^{19}	460	36)	97.92	17.6	0.21	3.5	1.56×10^{19}
						37)	52.65	22.0	0.11	3.5[*4]	1.45×10^{19}
						ave.	71.8	19.7	0.16	—	1.50×10^{19}
	12	2007 Niigata-Ken Chuuetsu-Oki	10)	9.30×10^{18}	537	38)	85.9	22.5	0.16	3.5[*4]	1.82×10^{19}
						39)	94.08	24.5	0.18	3.5[*4]	2.10×10^{19}
						ave.	89.9	23.5	0.17	—	1.95×10^{19}
	13	2008 Iwate-Miyagi Nairiku	10)	2.72×10^{19}	702	40)	92.48	13.8	0.13	3.5	1.15×10^{19}
						41)	85.64	17.6	0.12	3.5[*4]	1.42×10^{19}
						ave.	89.0	15.6	0.13	—	1.28×10^{19}
	14	2008 Wenchuan	5)	1.10×10^{21}	11,460	42)	1262.9	13.6	0.11	3.5[*4]	4.20×10^{19}
	15	2014 Ngano-Ken Hokubu	49)	2.76×10^{18}	263	43)	69.1	12.6	0.26	3.5	9.10×10^{18}
Normal	16	2011 Fukushima-Ken Hamadori	50)	9.58×10^{18}	640	44)	79	14.6	0.12	3.5[*4]	1.13×10^{19}
						total ave.	—	14.0	0.183	—	—

*1 M_0 : Seismic moment, S : Fault area

*2 Aftershock area

*3 S_{SMGA}, $\Delta\sigma_{SMGA}$: Area and Stress drop, β : S-wave velocity, A_{SMGA} : Short-period level *4 Assumed β

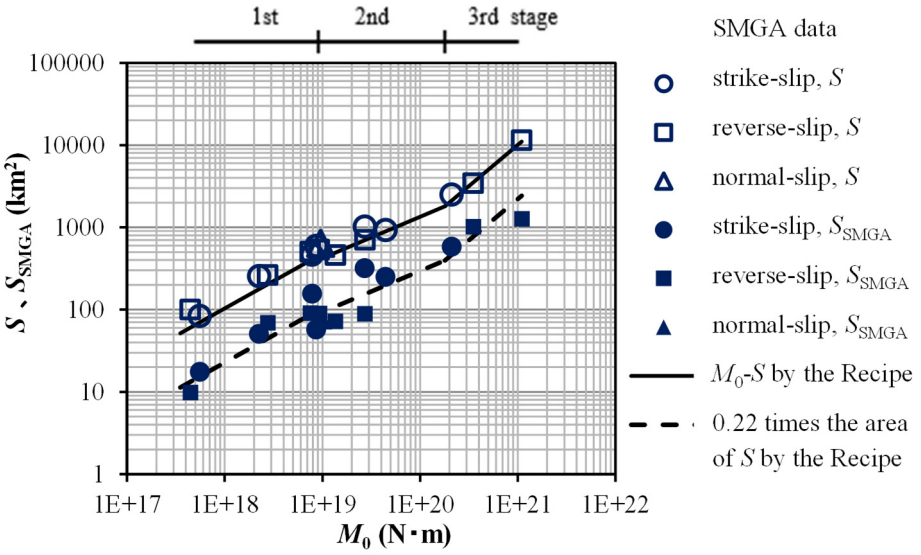

Fig. 4 M_0–S relationship between the seismic moment M_0 and fault area S, and the M_0–S_{SMGA} relationship between M_0 and area of the SMGA data S_{SMGA} listed in Table 1

assumed to be 3.5 km/s, which is the most common in the known data. Hereafter, when using the SMGA parameters listed in Table 1, which cites multiple references for earthquakes, the geometric mean of the parameters of multiple cited references is used.

Figure 4 depicts the relationship between M_0 and S in the data collected in Table 1. The solid line depicted in Fig. 4 exhibits the M_0–S relationship according to Eq. (1) of the three-stage model in the Recipe. The M_0–S relationship of the collected data is consistent with that of the three-stage model in the Recipe. Furthermore, the relationship between M_0 and S_{SMGA} of the SMGA data listed in Table 1 and the relationship indicated by the dashed lines of the area obtained by multiplying the fault area S according to Eq. (1) by 0.22 are compared, as depicted in Fig. 4. The M_0–S_{SMGA} relationship of the SMGA data listed in Table 1 is consistent with the dashed lines depicted in Fig. 4.

In the following, the parameters (A, S_{asp}, $\Delta\sigma_{asp}$) of the asperity model and the parameters (A_{SMGA}, S_{SMGA}, $\Delta\sigma_{SMGA}$) based on the SMGA model, which have a large influence on strong ground motions, are considered to be compatible, and both are compared later.

4.2 Comparison of the three-fold-line model and SMGA data

Figure 5 depicts the relationship between the seismic moment M_0 and short-period level A_{SMGA} obtained from the area and stress drop of the collected SMGA data. In Fig. 5, the relationship between M_0 and A obtained using Eq. (3) by Dan et al.[6] is indicated using a solid line and that of the three-fold-line model obtained using Eq. (10) in Section 3.3 is indicated using dashed lines. By comparing the M_0–A relationship by Eq. (3) and Eq. (10) with the M_0– A_{SMGA} relationship of the SMGA data, the M_0–A expressed in Eq. (3) and Eq. (10) are as well consistent as the M_0–A_{SMGA} of the SMGA data in $M_0 \leq 4.42\times10^{19}$ Nm below the upper limit of the data in the second stage. For the SMGA data of three overseas earthquakes in the range of 2.1×10^{20} Nm $\leq M_0$, the M_0–A relationship according to Eq. (10) corresponds better to the M_0–A_{SMGA} relationship of the SMGA data than that obtained using Eq. (3).

As the estimation accuracy of A using the empirical equations of Eq. (3) and Eq. (10) for the short-period level of the collected SMGA data A_{SMGA}, the ratios of A estimated by substituting M_0 into Eq. (3) or Eq. (10) to the A_{SMGA} of the SMGA data were obtained. Taking the geometric mean of these ratios

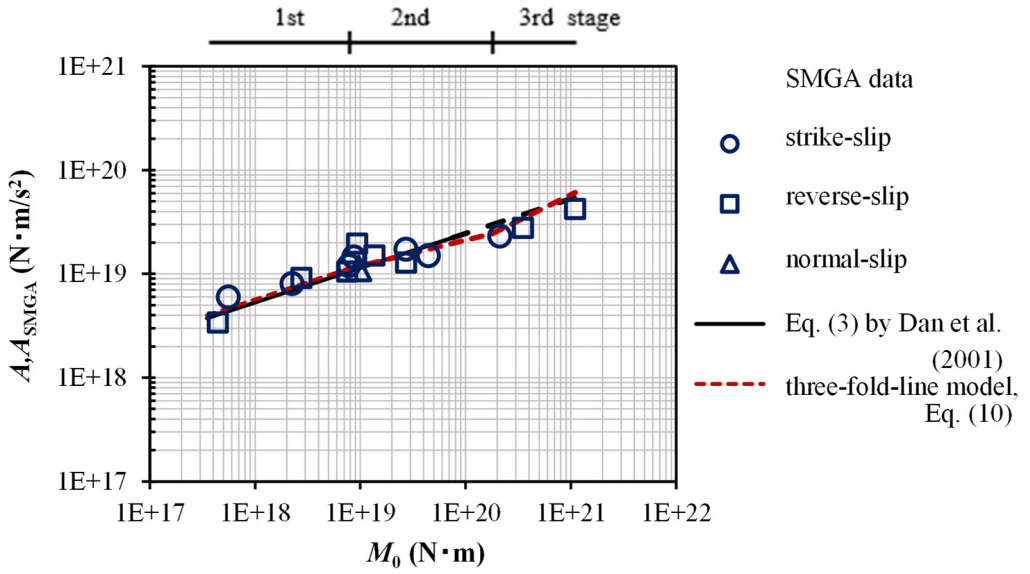

Fig. 5 M_0–A_{SMGA} relationship between the seismic moment M_0 and short-period level of the SMGA data A_{SMGA} listed in Table 1. The solid line indicates the relationship of M_0–A for the short-period level A in Eq. (3) as obtained by Dan et al.[6] , and the dashed lines indicate the M_0–A by Eq. (10) of the three-fold-line model.

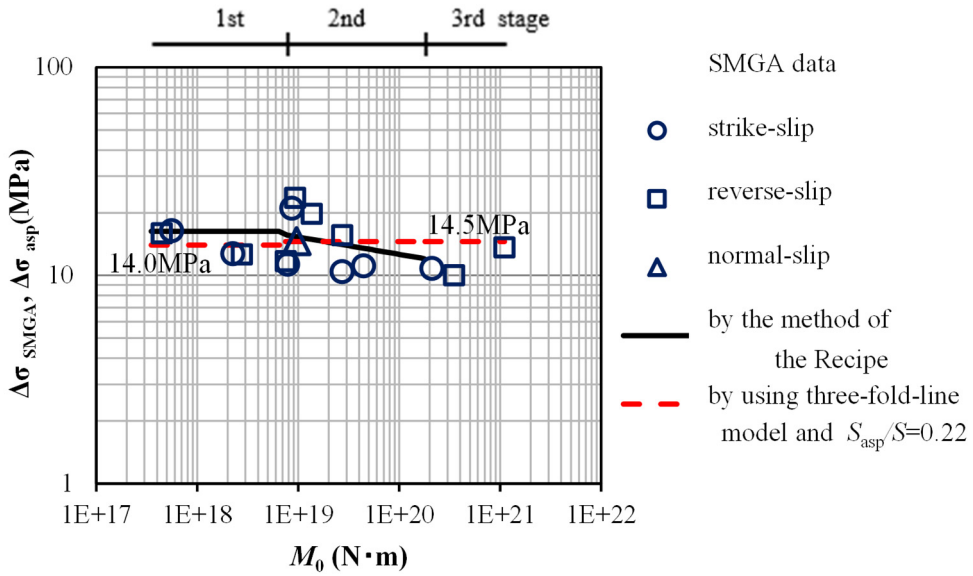

Fig. 6 The relationship M_0–$\Delta\sigma_{SMGA}$ between the seismic moment M_0 and the stress drop $\Delta\sigma_{SMGA}$ of the SMGA data listed in Table 1. The solid lines are the relationship of M_0–$\Delta\sigma_{asp}$ for the stress drop $\Delta\sigma_{asp}$ obtained by the method shown in Fig.1 of the Recipe, and the dashed lines are the M_0–$\Delta\sigma_{asp}$ obtained by using Eq. (10) of the three-fold-line model and the area ratio S_{asp}/S of 0.22.

from 16 earthquake data points, the average ratios, according to Eq. (3) and Eq. (10) were 0.97 and 0.99, respectively. The natural logarithmic standard deviations ζ of the ratios were 0.26 for Eq. (3) and 0.23 for Eq. (10), and the latter was slightly smaller. Here, the SMGA data were divided by fault type for strike-slip and longitudinal slip earthquakes, and the geometric means of ratios using Eq. (10) were 0.93 and 1.03, respectively. Thus, the difference in the short-period level A_{SMGA} for the SMGA data of strike-slip and longitudinal slip earthquakes was relatively small. This tendency is related to the difference in the area ratio and stress drop in the SMGA data, S_{SMGA}/S and $\Delta\sigma_{SMGA}$ as listed in Table 1, constituting the short-period level A in Eq. (4). For the area ratio S_{SMGA}/S, the mean of all data is 0.183 (ζ= 0.42), but the mean ratios of strike-slip and longitudinal slip data are 0.222 and 0.158, respectively, which indicates that the area ratio of strike-slip faults is larger. On the other hand, for the stress drop $\Delta\sigma_{SMGA}$, the mean of all data is 14.0 MPa (ζ = 0.28), but the means of strike-slip and longitudinal slip data are 13.0 MPa and 14.8 MPa, respectively, which indicates that the stress drop in the longitudinal slip fault is larger.

The dashed lines indicated in Fig. 6 are the stress drop of asperity to be 14.0 MPa, 14.5 MPa, and 14.5 MPa at each stage obtained using the short-period level A by Eq. (10) of the three-fold-line model and an area ratio of 0.22 in Section 3.4. In Fig. 6, they are compared with the SMGA data $\Delta\sigma_{SMGA}$. The solid lines in Fig. 6 show the relationship of M_0–$\Delta\sigma_{asp}$ obtained by Eq. (6) in the Recipe shown in Fig. 1, which is constant in the first stage and decreases to $M_0^{-1/12}$ in the second stage. While there are SMGA data for three earthquakes with a seismic moment M_0 of approximately 1.0×10^{19} Nm and a stress drop of approximately 20 MPa, $\Delta\sigma_{SMGA}$ of the other 13 earthquakes are almost constant with respect to the seismic moment. The stress drop $\Delta\sigma_{asp}$ obtained by using the three-fold-line model consistent with the characteristics of the stress drop $\Delta\sigma_{SMGA}$ in the SMGA data is slightly larger than $\Delta\sigma_{SMGA}$.

4.3 Comparison of the three-fold-line model and an empirical equation obtained from the SMGA data

Using the collected SMGA data of the seismic moment M_0 and short-period level A_{SMGA} listed in Table 1, the same scaling relationship of M_0–A_{SMGA} as in Eq. (9) was set, and the constants of the relationship were obtained using the least-squares method. Equation (13) is an empirical equation for the relationship

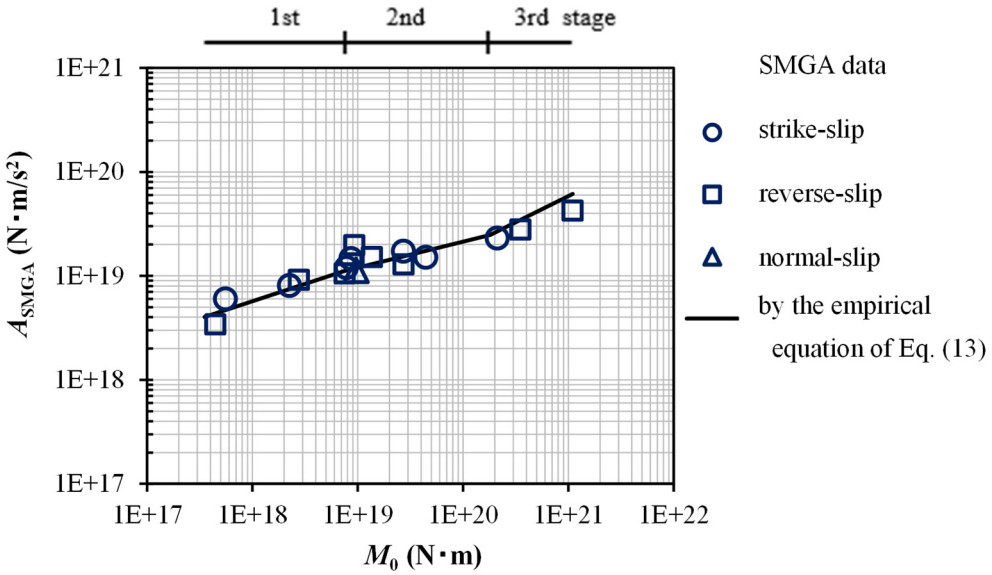

Fig. 7 M_0–A_{SMGA} relationship between the seismic moment M_0 and short-period level of the SMGA data A_{SMGA} listed in Table 1, and that by the empirical equation of Eq. (13)

between M_0 and A_{SMGA} in the first, second, and third stages, obtained for the relationship between the seismic moment (M_0; Nm) and the short-period level (A_{SMGA}; Nm/s^2).

$$A_{SMGA} = \begin{cases} 5.73\times10^{12}\times M_0^{1/3} & , \quad M_0 < 7.5\times10^{18} \\ 2.14\times10^{14}\times M_0^{1/4} & , \quad 7.5\times10^{18} \le M_0 \le 1.8\times10^{20} \\ 1.85\times10^{9}\times M_0^{1/2} & , \quad M_0 > 1.8\times10^{20} \end{cases} \tag{13}$$

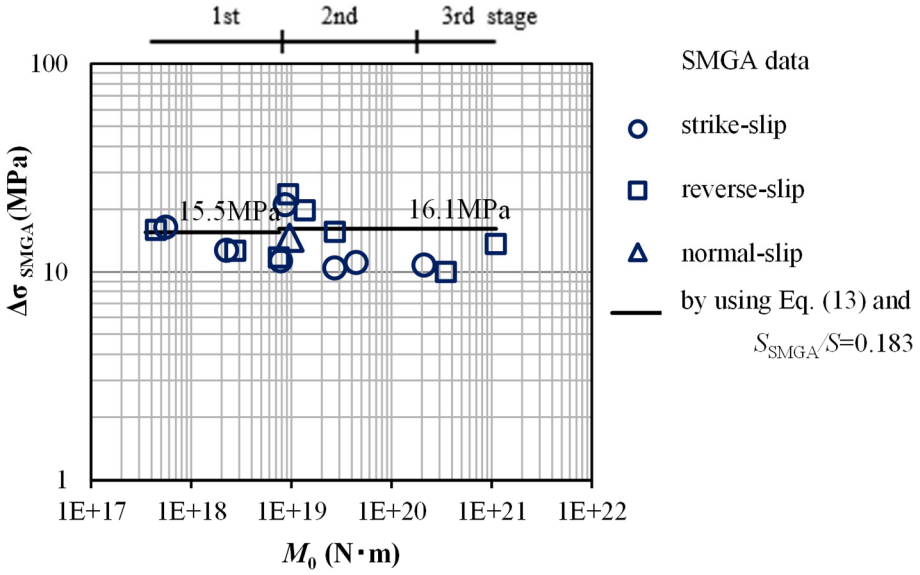

Fig. 8 M_0–$\Delta\sigma_{SMGA}$ relationship between the seismic moment M_0 and stress drop of the SMGA data $\Delta\sigma_{SMGA}$ listed in Table 1, and that obtained by using the empirical equation of Eq. (13) and the area ratio S_{SMGA}/S of 0.183

Figure 7 depicts a comparison of the relationship of M_0–A_{SMGA} using Eq. (13) with the SMGA data. The natural logarithmic standard deviation for error estimated by Eq. (13) was 0.23. The constants in Eq. (13) are 1.01 times the constants in Eq. (10), and Eq. (10) corresponds well with Eq. (13) obtained using the least-squares method from the SMGA data.

Next, using the relationship between M_0 and A_{SMGA} expressed by Eq. (13), the stress drop $\Delta\sigma_{SMGA}$ was determined using Eq. (11). Herein, for the fault area S in Eq. (11), the relationship between M_0 and S by Eq. (2) was applied. The area ratio s_{casp} in Eq. (11) is 0.183, which is the geometric mean of the area ratio S_{SMGA}/S of the SMGA data, and the shear wave velocity β is 3.46 km/s, which is the average of the SMGA data listed in Table 1. The constant stress drops $\Delta\sigma_{SMGA}$ obtained under these conditions in each stage were 15.5 MPa, 16.1 MPa, and 16.1 MPa, respectively. The stress drops $\Delta\sigma_{SMGA}$ were compared with the relationship of M_0–$\Delta\sigma_{SMGA}$ of the SMGA data depicted in Fig. 8. The 15.5 MPa, 16.1 MPa, and 16.1 MPa in each stage were larger than the geometric mean of $\Delta\sigma_{SMGA}$ from the SMGA data listed in Table 1, which was 14.0 MPa. These results are different from the stress drop $\Delta\sigma_{asp}$ when Eq. (10) and area ratio $S_{asp}/S = 0.22$ are used, which is relatively compatible with $\Delta\sigma_{SMGA}$ in the SMGA data shown in Fig. 6. Because the short-period levels of both are almost the same, it can be said that the difference of their stress drops is affected by the difference of the area ratio s_{casp} applied in Eq. (11). Therefore, the evaluation of the area ratio s_{casp} applied to set the area S_{SMGA} of the SMGA data will be an important issue in the future.

5. CONCLUSIONS

We re-examined the scaling law for the short-period level of the empirical equation by Dan et al.[6], which plays an important role in the evaluation of the asperity model of inland crustal earthquakes in the Recipe[1] by HERP to predict strong ground motions.

From the scaling law of the three-stage model on the relationship of M_0–S between the seismic moment M_0 and the fault area S in the Recipe, the fault area is scaled to $M_0^{2/3}$, $M_0^{1/2}$, and M_0^{1} in the first, second, and third stages, respectively; however, the empirical equation for short-period level A according to Dan et al.[6] is scaled to $M_0^{1/3}$ with a constant slope. In this study, we formulated a new relationship, M_0–A in which the short-period level A is scaled to $M_0^{1/3}$, $M_0^{1/4}$, and $M_0^{1/2}$ in each stage, as shown in Eq. (9), so that the area ratio and stress drop of the asperity become constant regardless of M_0 in each stage of the three-stage model. The constants of the new empirical equation for the short-period level in Eq. (9) were determined using the least-squares method by applying the same data as in Dan et al.[6]. Here, the relationship between M_0 and A using Eq. (10) is called the three-fold-line model for the short-period level. The three-fold-line model by Eq. (10) can explain the relationship of M_0–A of the earthquake data to the same extent as the empirical equation in Eq. (3) by Dan et al.[6]. Furthermore, when the area ratio of asperity, S_{asp}/S was set to 0.22 and the empirical equation of Eq. (10) was applied, the stress drops of asperity, $\Delta\sigma_{asp}$ in the first, second, and third stages were 14.0 MPa, 14.5 MPa, and 14.5 MPa in each stage to be constant regardless of M_0.

Next, we collected data on the area S_{SMGA} and stress drop $\Delta\sigma_{SMGA}$ of the strong motion generation area (SMGA), which is considered equivalent to the asperity parameters for inland crustal earthquakes, obtained from strong ground motion simulations of observation records. Using their parameters, the short-period level A_{SMGA} of the SMGA data was obtained. By comparing the M_0–A relationship of the three-fold-line model using Eq. (10) with the M_0–A_{SMGA} relationship of the SMGA data, we showed that both the relationships are good correspondence in the range of 4.44×10^{17} Nm $\leq M_0 \leq 1.10\times10^{21}$ Nm of the SMGA data from the first stage to the third stage.

As described above, it was found that the three-fold-line model for the short-period level by Eq. (10), which reconsider the scaling law, is consistent with the characteristics of the collected earthquake observation records. However, because there are few earthquake data for long faults, it is necessary to accumulate such data and examine the three-fold-line model using Eq. (10).

In addition, the asperity region of the fault with an area ratio S_{asp}/S of 0.22 applied in Section 3.4, directly indicates a fault area with a large slip extracted from the heterogeneous slip distribution obtained by the seismic source inversion in the long period range. Based on previous research, we considered this

area to have a large stress drop and to be equivalent to the area where strong motions are generated, including shorter periods. However, the SMGA is a strong motion generation area with a large stress drop, as estimated by the simulation analyses of earthquake observation records using the empirical Green's function method, which mainly focuses on the short-period range. Thus, the degree of accuracy at which the asperity and SMGA match the different periodic ranges and analysis methods used for extraction is considered to be one of the issues to be examined in the future, considering recent improvements in the accuracy of long-period waveform inversion and the expansion of applicability to a shorter period range. Based on these studies, it is important to accurately evaluate the area ratio $s_{casp} = S_{asp}/S$ of asperity, which can be used to set an appropriate asperity area S_{asp} corresponding to Eq. (11) for obtaining the stress drop $\Delta\sigma_{asp}$ of asperity, in order to improve the future strong ground motion prediction.

In the future, we will examine the above problems and construct a method for evaluating the parameters (S_{asp}, $\Delta\sigma_{asp}$) of the asperity model based on the theoretical formula of Eq. (4) using the scaling relation for the short-period level associated with the three-stage model developed in this study.

ACKNOWLEDGMENT

This research is a part of the results obtained in the research project of "Support Work for National Seismic Hazard Maps for Japan" by National Research Institute for Earth Science and Disaster Resilience (NIED). We express our sincere gratitude to Dr. Asako Iwaki (NIED) for her useful opinions in compiling this research. We would also like to thank three anonymous reviewers for their valuable comments.

REFERENCES

1) Headquarters for Earthquake Research Promotion: Strong Ground Motion Prediction Method for Earthquakes with Specified Source Faults ("Recipe"), 2020 (in Japanese). https://www.jishin.go.jp/main/chousa/20_yosokuchizu/recipe.pdf (last accessed on January 6, 2022)
2) Irikura, K. and Miyake, H.: Recipe for Predicting Strong Ground Motion from Crustal Earthquake Scenarios, *Pure and Applied Geophysics*, No. 168, pp. 85–104, 2011.
3) Somerville, P. G., Irikura, K., Graves, R., Sawada, S., Wald, D., Abrahamson, N., Iwasaki, Y., Kagawa, T., Smith, N. and Kowada, A.: Characterizing Crustal Earthquake Slip Models for the Prediction of Strong Ground Motion, *Seismological Research Letters*, Vol. 70, No. 1, pp. 59–80, 1999.
4) Irikura, K. and Miyake, H.: Prediction of Strong Ground Motions for Scenario Earthquakes, *Journal of Geography*, Vol. 110, 849–875, 2001 (in Japanese with English abstract).
5) Murotani, S., Matsushima, S., Azuma, T., Irikura, K. and Kitagawa, S.: Scaling Relations of Source Parameters of Earthquakes Occurring on Inland Crustal Mega-Fault Systems, *Pure and Applied Geophysics*, No. 172, pp. 1371–1381, 2015.
6) Dan, K., Watanabe, M., Sato, T. and Ishii, T.: Short-Period Source Spectra Inferred from Variable-Slip Rupture Models and Modeling of Earthquake Faults for Strong Motion Prediction by Semi-Empirical Method, *Journal of Structural and Construction Engineering* (*Transactions of the Architectural Institute of Japan*), No. 545, pp. 51–62, 2001 (in Japanese with English abstract).
7) Dan, K., Ju, D., Irie, K., Arzpeima, S. and Ishii, Y.: Estimation of Averaged Dynamic Stress Drops of Inland Earthquakes Caused by Long Strike-Slip Faults and Its Application to Asperity Models for Predicting Strong Ground Motions, *Journal of the Structural and Construction Engineering* (*Transactions of the Architectural Institute of Japan*), No. 670, pp. 2041–2050, 2011 (in Japanese with English abstract).
8) Tajima, R., Matsumoto, Y., Si, H. and Irikura, K.: Comparative Study on Scaling Relations of Source Parameters for Great Earthquakes in Inland Crusts and on Subducting Plate-Boundaries, *Zisin* (*Journal of the Seismological Society of Japan*), Vol. 66, pp. 31–45, 2013 (in Japanese with

English abstract).
9) Nagashima, F., Kawase, H. and Ito, E.: Investigation of Scaling Relations by Using Database Composed of Inversion Models of Inland Crustal Earthquakes in Foreign Countries, *Journal of Japan Association for Earthquake Engineering*, Vol. 21, No. 5, pp. 140–160, 2021 (in Japanese with English abstract).
10) Miyakoshi, K., Irikura, K. and Kamae, K.: Re-Examination of Scaling Relationships of Source Parameters of the Inland Crustal Earthquakes in Japan Based on the Waveform Inversion of Strong Motion Data, *Journal of Japan Association for Earthquake Engineering*, Vol. 15, No. 7, pp. 141–156, 2015 (in Japanese with English abstract).
11) Miyakoshi, K., Somei, K., Yoshida, K., Kurahashi, S., Irikura, K. and Kamae, K.: Scaling Relationships of Source Parameters of Inland Crustal Earthquakes in Tectonically Active Regions, *Pure and Applied Geophysics*, No. 177, pp. 1917–1929, 2020.
12) Miyake, H., Iwata, T. and Irikura, K.: Source Characterization for Broadband Ground-Motion Simulation: Kinematic Heterogeneous Source Model and Strong Motion Generation Area, *Bulletin of the Seismological Society of America*, Vol. 93, pp. 2531–2545, 2003.
13) Tohdo, M., Ju, D., Fujiwara, H. and Morikawa, N.: Study on the Averaged Stress Drop, and Area and Stress Drop of Asperity from Crustal Earthquake Data, *Summaries of Technical Papers of Annual Meeting, Architectural Institute of Japan,* Structures B-2, pp. 255–256, 2021 (in Japanese).
14) Dan, K., Irie, K., Ju, D., Shimazu, N and Torita, H.: Procedure for Estimating Parameters of Fault Models of Inland Earthquakes Caused by Long Reverse Faults, *Journal of the Structural and Construction Engineering* (*Transactions of the Architectural Institute of Japan*) , No. 707, pp. 45–57, 2015 (in Japanese with English abstract).
15) Hikima, K. and Shimmura, A.: Moment-Area Scaling Relationship Assuming Constant Stress Drop for Crustal Earthquakes, *Bulletin of the Seismological Society of America*, Vol. 110, pp. 241–249, 2020.
16) Hikima, K. and Shimmura, A.: Source Parameters for Strong Motion Prediction Using Moment-Area Scaling with Constant Stress Drop for Crustal Earthquakes, *Summaries of Technical Papers of Annual Meeting, Architectural Institute of Japan*, Structures B-2, pp. 457–458, 2019 (in Japanese).
17) Dan, K., and Sato, T.: Strong-Motion Prediction by Semi-Empirical Method Based on Variable-Slip Rupture Model of Earthquake Fault, *Journal of the Structural and Construction Engineering* (*Transactions of the Architectural Institute of Japan*), No. 509, pp. 49–60, 1998 (in Japanese with English abstract).
18) Brune, J. N.: Tectonic Stress and the Spectra of Seismic Shear Waves from Earthquakes, *Journal of Geophysical Research*, Vol. 75, No. 26, pp. 4997–5009, 1970.
19) Boatwright, J.: The Seismic Radiation from Composite Models of Faulting, *Bulletin of the Seismological Society of America*, Vol. 78, pp. 489–508, 1988.
20) Eshelby, J. D.: The Determination of the Elastic Field of an Ellipsoidal Inclusion, and Related Problems, *Proceedings of the Royal Society of London*, Series A, Vol. 241, pp. 376–396, 1957.
21) Madariaga, R.: On the Relation between Seismic Moment and Stress Drop in the Presence of Stress and Strength Heterogeneity, *Journal of Geophysical Research*, Vol. 84, No. B5, pp. 2243–2250, 1979.
22) Fujii, Y. and Matsu'ura, M.: Regional Difference in Scaling Laws for Large Earthquakes and Its Tectonic Implication, *Pure and Applied Geophysics*, No . 157, pp. 2283–2302, 2000.
23) Kamae, K. and Irikura, K.: A Fault Model of the 1995 Hyogo-Ken Nanbu Earthquake and Simulation of Strong Ground Motion in Near-Source Area, *Journal of the Structural and Construction Engineering* (*Transactions of the Architectural Institute of Japan*), No. 500, pp. 29–36, 1997 (in Japanese with English abstract).
24) Hirai, T., Kamae, K., Naganuma, T., Ito, S., Nishioka, T. and Irikura, K.: Simulation of Strong Ground Motion due to the 1995 Hyogo-Ken Nanbu Earthquake by Using Characterized Source Model with Branch Fault, *Journal of Japan Association for Earthquake Engineering*, Vol. 6, No. 3, pp. 2–11, 2006 (in Japanese with English abstract).
25) Kamae, K. and Irikura, K.: Source Characterization and Strong Motion Simulation for the 1999 Kocaeli, Turkey and the 1999 Chi-Chi, Taiwan Earthquakes, *Proceedings of the 11th Japan*

Earthquake Engineering Symposium, pp. 545–550, 2002 (in Japanese with English abstract).
26) Ikeda, T., Kamae, K., Miwa, S. and Irikura, K.: Source Characterization and Strong Ground Motion Simulation of the 2000 Tottori-Ken Seibu Earthquake Using the Empirical Green's Function Method, *Journal of the Structural and Construction Engineering* (*Transactions of the Architectural Institute of Japan*) , No. 561, pp. 37–45, 2002 (in Japanese with English abstract).
27) Satoh, T. and Kawase, H.: Estimation of Characteristic Source Model of the 2005 West Off Fukuoka Prefecture Earthquake Based on Empirical Green's Function Method, *Proceedings of the 12th Japan Earthquake Engineering Symposium*, pp. 170–173, 2006 (in Japanese with English abstract).
28) Somei, K., Miyakoshi, K. and Irikura, K. : Source Model and Strong Ground Motion Simulation for the 2013 Northern Tochigi Prefecture, Japan, Eearthquake, *Japan Geoscience Union Meeting*, SSS23-P19, 2014 (in Japanese).
29) Irikura, K., Miyakoshi, K., Kamae, K., Yoshida, K., Somei, K., Kurahashi, S. and Miyake, H.: Applicability of Source Scaling Relations for Crustal Earthquakes to Estimation of the Ground Motions of the 2016 Kumamoto Earthquake, *Earth, Planets and Space*, Vol. 69, 2017. https://doi.org/10.1186/s40623-016-0586-y
30) Satoh, T.: Broadband Source Characteristics of the 2016 Kumamoto Earthquake Estimated from Strong Motion Records, *Journal of the Structural and Construction Engineering (Transactions of the Architectural Institute of Japan)*, No. 741, pp. 1707–1717, 2017 (in Japanese with English abstract).
31) Oana, A., Dan, K., Miyakoshi, J., Fujiwara, H., Morikawa, N. and Maeda, T.: Estimation of Characterized Source Model of the Mainshock in the 2016 Kumamoto Earthquakes Using the Stochastic Green's Function Method, *Japan Geoscience Union Meeting*, SCG70-P04, 2017 (in Japanese).
32) Yoshida, S., Kagawa, T. and Noguchi, T.: Characterized Seismic Source Model for the 2016 Central Tottori Earthquake Using Empirical Green's Function Method, *Journal of the Japan Association for Earthquake Engineering*, Vol. 18, No. 2, pp. 51–61, 2018.
33) Kamae, K., Ikeda, T. and Miwa, S.: Source Model Composed of Asperities for the 2004 Mid Niigata Prefecture, Japan, Earthquake (M_{JMA} = 6.8) by the Forward Modeling Using the Empirical Green's Function Method, *Earth, Planets and Space*, Vol. 57, pp. 533–538, 2005.
34) Satoh, T., Hijikata, K., Uetake, T., Tokumitsu, R. and Dan,K.: Cause of Large Peak Ground Acceleration of the 2004 Niigata-Ken Chuetsu Earthquake by Broadband Source Inversion, *Summaries of Technical Papers of Annual Meeting, Architectural Institute of Japan*, Structures B-2, pp. 365–366, 2007 (in Japanese).
35) Maeda, T. and Sasatani, T.: Strong Ground Motions from an M_j 6.1 Inland Crustal Earthquake in Hokkaido, Japan: the 2004 Rumoi Earthquake, *Earth, Planets and Space*, Vol. 61, pp. 689–701, 2009.
36) Kamae, K., Ikeda, T. and Miwa, S.: Source Model of the 2007 Noto-Hanto Earthquake (M_J 6.9), 2007 (in Japanese, title translated by the authors). http://www.rri.kyoto-u.ac.jp/jishin/eq/notohantou/notohantou.html (last accessed on October 20, 2020)
37) Kurahashi, S., Masaki, K. and Irikura, K.: Source Model of the 2007 Noto-Hanto Earthquake (M_w 6.7) for Estimating Broad-Band Strong Ground Motion, *Earth, Planets and Space*, Vol. 60, pp. 89–94, 2008.
38) Kurahashi, S., Masaki, K., Miyakoshi, K and Irikura, K.: Source Model of the 2007 Niigata-Ken Chuuetsu-Oki Earthquake Using Empirical Green's Function (SE-Dip Model), *Japan Geoscience Union Meeting*, S146-P017, 2008 (in Japanese).
39) Kamae, K. and Kawabe, H.: Source Model of the 2007 Niigata-Ken Chuuetsu-Oki Earthquake (M_j 6.8) and Simulation of Strong Ground Motion, 2008 (in Japanese, title translated by the authors). http://www.rri.kyoto-u.ac.jp/jishin/eq/niigata_chuetsuoki_5/chuuetsuoki_20080307.pdf (last accessed on October 20, 2020)
40) Kamae, K.: Source Model of the 2008 Iwate-Miyagi Nairiku Earthquake (M_j 7.2), 2008 (in Japanese, title translated by the authors). http://www.rri.kyoto-u.ac.jp/jishin/iwate_miyagi_1.html (last accessed on October 20, 2020)
41) Irikura, K. and Kurahashi, S.: Source Model of the 2008 Iwate-Miyagi Nairiku Earthquake and

Strong Ground Motions (Cause of Large Peak Ground Acceleration), *Annual Meeting of Japanese Society for Active Fault Studies*, 2008 (in Japanese, title translated by the authors). http://www.kojiro-irikura.jp/pdf/katudansougakkai2008.pdf (last accessed on October 20, 2020)
42) Kurahashi, S. and Irikura, K.: Characterized Source Model for Simulating Strong Ground Motions during the 2008 Wenchuan Earthquake, *Bulletin of the Seismological Society of America*, Vol. 100, pp. 2450–2475, 2010.
43) Ikeda, T., Konagai, K., Kamae, K., Sato, T. and Takase, Y.: Damage Investigation and Source Characterization of the 2014 Northern Part of Ngano Prefecture Earthquake, *Journal of Japan Society of Civil Engineers*, Ser. A1, Vol. 72, No. 4, pp. 975–983, 2016 (in Japanese with English abstract).
44) Somei, K., Miyakoshi, K. and Irikura, K.: Estimation of Source Model and Strong Motion Simulation for the 2011 East Fukushima Prefecture Earthquake Using the Empirical Green's Function Method, *Program and Abstracts, the Seismological Society of Japan*, P2-29, 2011 (in Japanese).
45) Iwata, T. and Sekiguchi, H.: Source Model of the 2000 Tottori-Ken Seibu Earthquake and Near-Source Strong Ground Motion, *Proceedings of the 11th Japan Earthquake Engineering Symposium*, pp. 125–128, 2002 (in Japanese with English abstract).
46) Asano, K. and Iwata, T.: Source Process and Near-Source Ground Motions of the 2005 West Off Fukuoka Prefecture Earthquake, *Earth, Planets and Space*, Vol. 58, pp. 93–98, 2006.
47) Kubo, H., Suzuki, W., Aoi, S. and Sekiguchi, H.: Source Rupture Process of the 2016 Central Tottori, Japan, Earthquake (M_{JMA} 6.6) Inferred from Strong Motion Waveforms, *Earth, Planets and Space*, Vol. 69, 2017. https://doi.org/10.1186/s40623-017-0714-3
48) Asano, K. and Iwata, T.: Source Rupture Process of the 2004 Chuetsu, Mid-Niigata Prefecture, Japan, Earthquake Inferred from Waveform Inversion with Dense Strong-Motion Data, *Bulletin of the Seismological Society of America*, Vol. 99, pp. 123–140, 2009.
49) Kurahashi, S., Irikura, K. and Miyakoshi, K.: Characterized Source Model for Estimating Broad-Band Strong Ground Motions during the 2014 Northern Nagano Earthquake, *Program and Abstracts, the Seismological Society of Japan*, S15-P04, 2016 (in Japanese).
50) Hikima, K.: Rupture Process of the April 11, 2011 Fukushima Hamadori Earthquake, (M_j 7.0), *Zisin* (*Journal of the Seismological Society of Japan*), Vol. 64, pp. 243–256, 2012 (in Japanese with English abstract).

Original Japanese Paper Published: November, 2022)
(English Version Submitted: October 4, 2023)
(English Version Accepted: November 11, 2023)